Journal of Molecular Structure 1294 (2023) 136340

Contents lists available at ScienceDirect

Journal of Molecular Structure

journal homepage: www.elsevier.com/locate/molstr

The peculiar SHG behaviour of Co-5,10,15,20-tetraphenilporphyrinate in the solid state. An experimental and theoretical study

Paola Antoniotti [a,b,*], Carlo Canepa [a], Elena Cariati [c], Alma Cioci [a], Enzo Laurenti [a], Domenica Marabello [a,b], Giorgio Volpi [a], Paola Benzi [a,b]

[a] Dipartimento di Chimica, University of Torino, Torino, Italy
[b] Crisdi – Interdepartmental Center for Crystallography, University of Torino, Torino, Italy
[c] Dipartimento di Chimica, University of Milano, Milano, Italy

ARTICLE INFO

Keywords:
Metal porphyrinates
SHG properties
Theoretical calculations
NLO properties
Structure-properties relashionship

ABSTRACT

We prepared and investigated the SHG behavior in the solid state of the Cobalt 5,10,15,20-tetraphenylporphyrinate that crystallizes in the acentric $I\bar{4}2d$ space group. The compound was synthesized and characterized, and the Second Harmonic Generation (SHG) response of a powdered sample was measured through a 1.907 μm pulsed laser radiation. During laser irradiation, a gradual increase of the intensity of the SH signal was observed until, after a few minutes, it reached a plateau of about fifty times the initial value. We attempted to understand the origin of this peculiar SHG behavior, both through experimental analysis and theoretical calculations. Mass spectrometry, absorption, emission, and vibrational spectroscopies in solution combined with powder X-ray diffraction analysis in solid state, both before and after irradiation, do not evidence any chemical degradation, phase transition or amorphization process. Theoretical calculations on little fragments of the Co-TPP structure simulate appropriately the structural feature of the complex and its initial experimental SHG response. UV–VIS and EPR spectra collected in the solid state before and after irradiation, in conjunction with DFT/B3LYP optimization of excited spin states and TDDFT calculation, highlight a change in the electronic and/or spin state due to the irradiation of the complex.

1. Introduction

Porphyrins are heterocyclic macrocyclic organic compounds, much studied for numerous applications, due to their optical properties and chemical stability [1,2]. Due also to their biocompatibility and their remarkable fluorescence, they have been investigated for a long time as biosensors [3–6]. Among the optical properties, porphyrins show interesting Non Linear Optical (NLO) Properties, i.e. Second (SHG) and Third (THG) Harmonic Generation [7–11], in solution or encapsulated in polymers [12], and were recently investigated for NLO bio-imaging [13,14]. In fact, porphyrins are organic materials with prominent π-electron delocalization, that can achieve a significant enhancement of hyperpolarizability, by metal insertion at the ring center or functionalization at the peripheral positions [15].

Pizzotti et al. [16] investigated the SHG response in solution of a wide range of push-pull porphyrins, functionalized with electron-donating or electron-withdrawing groups in β-pyrrolic or in *meso* position, either as free bases or as Ni(II), Cu(II) or Zn(II) complexes [17–19]. It was demonstrated that the second order NLO property of porphyrins is due to a charge-transfer process between the porphyrin core and its substituents. Moreover, it was shown that in solution the SHG response is not affected by the nature of the metal, but by its capability to interact with other species in the free axial position, such as the solvent molecules.

Many interesting works about the SHG responses of porphyrins and their derivatives are present in the literature [20,21]. However, to our knowledge, up to now the SHG properties of porphyrins or their derivatives were not investigated in the solid state. In our recent works, we investigated the solid state, with experimental and computational methods, the SHG property of some crystalline metal-sugar derivatives, in order to exploit these solid materials as nano-biosensors [22–24]. In order to better correlate the second harmonic emission with the nature and structure of the material, computational models were used in which the crystalline fragment is represented as a macromolecule with

* Corresponding author at: Dipartimento di Chimica, University of Torino, Torino, Italy.
E-mail address: paola.antoniotti@unito.it (P. Antoniotti).

https://doi.org/10.1016/j.molstruc.2023.136340
Received 30 May 2023; Received in revised form 18 July 2023; Accepted 1 August 2023
Available online 5 August 2023

nanoparticle size. The geometrical parameters were optimized and compared with the experimental X-ray data, and the first-order static hyperpolarizability and second-order susceptibility were also calculated and compared with the values obtained for the sucrose used as a reference. The ratios obtained were compared with the experimentally measured SHG intensity ratios and the good agreement encouraged us to apply the same method to other molecular compounds.

In this work, we decided to investigate the SHG behavior of the Co-derivative of 5,10,15,20-tetraphenylporphyrin (H_2TPP, scheme 1a) in the solid state. A fundamental requirement for the presence in a solid material of the SHG property is the absence of the inversion center in the crystal structure and also eschew some special combination of symmetry elements [25]. Some metal porphyrinates, despite their molecular C_4 symmetry in solution, crystallize in non-centrosymmetric space groups. Among them, the Cobalt-5,10,15,20-tetraphenylporphyrinate of formula Co-TPP (scheme 1b), crystallizes in the acentric space group $I\bar{4}2d$, which suggests the possibility to observe a significant SHG emission.

Thus, we synthesized and characterized the Co-TPP with single crystal (XRD) and powder (XRPD) X-ray diffraction. We measured the SHG response of powdered samples with a 1.907 μm pulsed laser radiation, and, during laser irradiation, a gradual enhancement of the intensity of the SH signal was observed, and after few minutes, a plateau at a value about fifty times with respect to the initial one, was reached. By repeating the measurement on the same spot, a stable SHG signal of fifty times of the initial one was measured. To verify if this behavior is related to phase transition or photodegradation phenomena, the sample was analyzed with mass-spectrometry, absorption-, emission- and vibrational-spectroscopies, and powder X-ray diffraction (XRPD) both before and after irradiation.

UV–VIS and EPR analysis were also performed in the solid state, before and after irradiation, to verify changes in the electronic structure of the complex and/or spin state due to the irradiation of the complex. Moreover, theoretical calculations were performed at the B3-LYP/6–31G(d) level of theory on fragments consisting of two or three porphyrinate rings, in order to simulate appropriately the structure of a nanoparticle. Theoretical calculations were applied to fragments in order to estimate the first-order static hyperpolarizability and second-order susceptibility, which are correlated to the SHG response. To further explain the reason for the large increase of the SH signal after irradiation, the TDDFT method was used to describe the excited states and the results were compared to the electronic spectra of the complex before and after irradiation. Moreover, optimizations of some excited spin states were performed, to evaluate the variation of the hyperpolarizability as a function of the electronic and/or spin state and compare it to the experimental SHG data.

2. Experimental

2.1. Synthesis of Cobalt(II) 5,10,15,20-tetraphenilporphyrinate (Co-TPP)

All solvents and raw materials were used as received from commercial suppliers (Sigma-Aldrich and Alfa Aesar) without further purification.

H_2TPP and Co-TTP were synthesized according to the method reported by Girolami et al. [26]. The powder obtained was purified by dissolution in dichloromethane and re-crystallization through partial evaporation of the solvent. The crystalline powder was filtered and then washed with few drops of dichloromethane. The purity of the compound was checked through mass-spectrometry, absorption-, emission- and vibrational- spectroscopies, and powder X-ray diffraction (XRPD) (Figs. S4–S13 in Supporting Information).

2.2. Single crystal X-ray diffraction (XRD)

The crystal suitable for XRD was obtained by slow evaporation of the dichloromethane solution. X-ray diffraction data were collected at room temperature using the Atlas S2 Rigaku-Oxford Diffraction Gemini R-Ultra diffractometer equipped with graphite monochromatized Mo-Kα (0.71073 Å) radiation. The CrysAlisPro package [27] was used for data collection and integration, SHELXT [28] for resolution, SHELXL [29] for refinement and Olex2 [30] for graphics. Hydrogen atoms were found in the difference Fourier maps, nevertheless they were calculated and refined with riding coordinates and fixed U_{iso}at 1.2 times of the U_{eq} of the connected C atoms. The interested reader can find further details on crystal data, data collection, least-squares refinements and CIF files (CCDC 2,130,187) in the Supporting Information (Tables S1, S2, Figs. S1–S3).

2.3. Powder X-ray diffraction (XRPD)

The Powder X-ray diffraction patterns (XRPD) were collected with the same diffractometer of the XRD data collection, using the mirror monochromatized Cu-Kα (1.5418 Å) radiation. The powders were prepared by mixing 3.00 mg of each Co-TPP sample with 0.50 mg of ZnO and the solid mixture was ground in an agate mortar. The powders were compacted with paraffin oil and modelled as a ball of ca. 0.45 mm diameter (less than the diameter of the X-ray beam). Each ball was glued on a glass capillary and mounted on the goniometer head of the instrument. Each powder pattern was collected by rotating the samples 60°, and with an exposure time of 60 s.

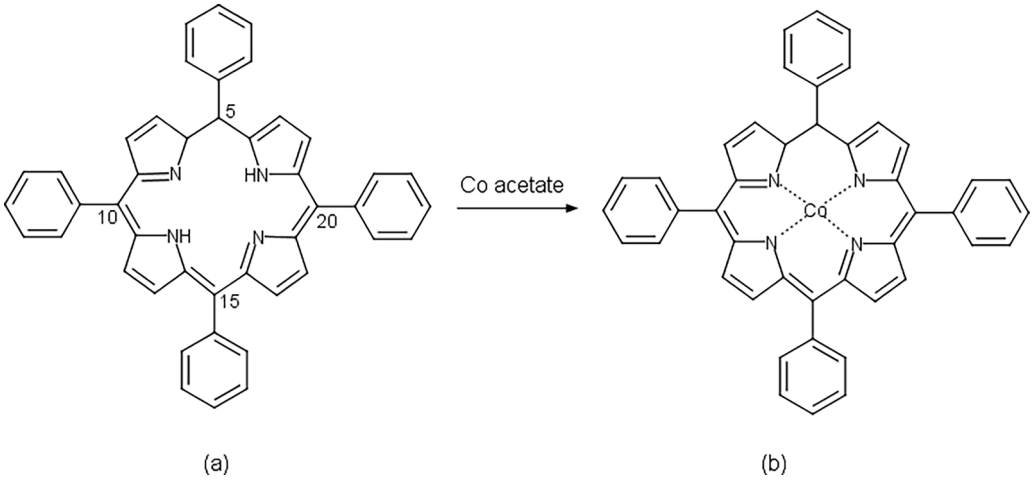

Scheme 1. Chemical scheme of 5,10,15,20-tetraphenylporphyrin (a) and Cobalt-5,10,15,20- tetraphenylporphyrinate (b).

Table 1
Absorption and emission maxima (nm) recorded in dichloromethane solution for H_2TPP and Co-TPP.

		H_2TPP	Co-TPP
Absorption	Soret bands (B band)	419	410
	Q bands	513	527
		549	612
		590	
		647	
Emission		652	649
		717	713
			792

2.4. Mass spectrometry and absorption, emission and vibrational spectroscopies

For the optical characterization of the Co-TPP complex, Photoemission spectra were recorded with a HORIBA Jobin Yvon IBH Fluorolog-TCSPC spectrofluorimeter and UV–Vis absorption spectra were recorded on a Cary60 spectrometer using dichloromethane solutions (10^{-5} M). Moreover, diffuse reflectance UV–Vis spectra of the powdered CoTPP and H_2TPP were recorded by an Agilent Cary 100 UV–Vis spectrophotometer equipped with an integration sphere. Vibrational spectra were recorded on powder samples on a Spectrum Two FT-IR Spectrometer PerkinElmer. Mass spectra were recorded on a Thermo-Finnigan Advantage Max Ion Trap Spectrometer equipped with an electrospray ion source (ESI), both in positive and negative ion acquiring mode.

2.5. Magnetic balance and electron paramagnetic resonance (EPR)

Magnetic susceptibility measurements were carried out with the Johnson Matthey Magnetic susceptibility Balance using Evans' method. EPR spectra of solid Co-TPP before and after irradiation were recorded at 77 K in a X-band Bruker-EMX instrument equipped with a cylindrical cavity operating at 100 kHz field modulation (microwave frequency 9.3 GHz, microwave power 10 mW, modulation amplitude 6 Gauss).

2.6. Computational methods

The calculations were performed with the GAUSSIAN16 program [31]. All the geometries in this work were optimized by gradient-based techniques [32–34] with no symmetry constraints at the DFT B3LYP level of theory [35,36], in conjunction with the 6–31G(d) basis set for the C, H, N atoms [37]. For Co the LANL2DZ basis was used [38]. All critical points were characterized as energy minima by calculating their analytical frequencies. The total dipole moment, polarizability and the first order hyperpolarizability were calculated at the same level of theory. Since ab initio volume calculations based on numerical Monte Carlo integration introduce a large degree of error. To compute the molar volume in a more quantitative way, tight convergence in the self-consistent field procedure and increased density of points for more accurate integration were employed, and ten different volume calculations on the optimized geometries at the B3LYP level of theory with the options scf=tight, volume=tight, and iop(6/45=500,6/46=1) were averaged [39]. To explain the SH behavior of the irradiated complex, we employed time-dependent density functional theory (TD-DFT) [40,41] with the same functional and basis set used for describing the excited states. The spectra were compared to the electronic spectra of the complex both before and after irradiation.

2.7. SHG measurements

The SHG efficiency was determined by the Kurtz–Perry powder technique [42], using a nanosecond Nd:YAG pulsed (10 Hz) laser whose 1.064 μm fundamental wavelength was shifted to 1.907 μm by stimulated Raman scattering in a high-pressure hydrogen cell. The SH signal generated by ground samples in capillary tubes was collected by an elliptical mirror, detected by a photomultiplier, and compared to the ground sucrose signal collected in the same conditions (sucrose displays an SHG equal to 0.7 that of KDP in the same conditions).

3. Results and discussion

In order to understand the reason of the peculiar SHG behavior of the Co-TPP after a few minutes of irradiation with the Nd:YAG pulsed laser, it was analyzed before and after irradiation with different analytical

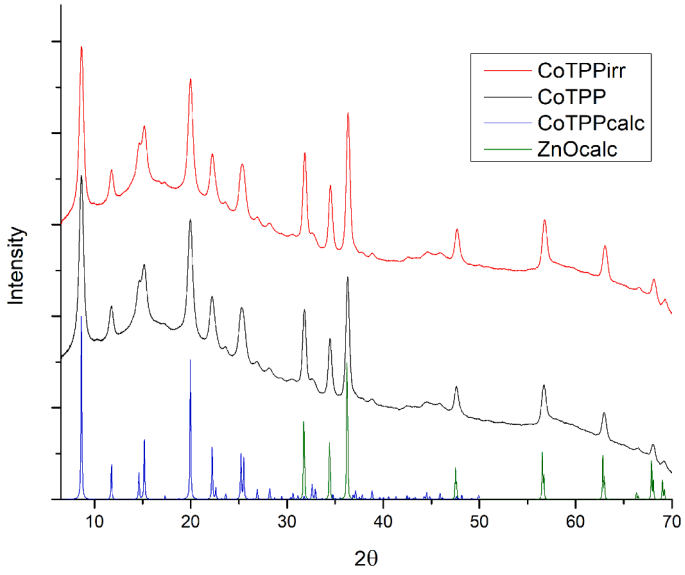

Fig. 1. XRPD patterns of powders of cobalt-porphyrinate both before (CoTPP) and after (CoTPPirr) irradiation with the Nd:YAG pulsed laser, mixed with those of ZnO, compared to the XRPD patterns calculated from the XRD structure (Co-TPPcalc), and to the ZnO pattern calculated for the $P6_3mc$ structure from the ICSD databank (ZnOcalc). The patterns of the CoTPP powders are scaled on the peaks' intensity of ZnO.

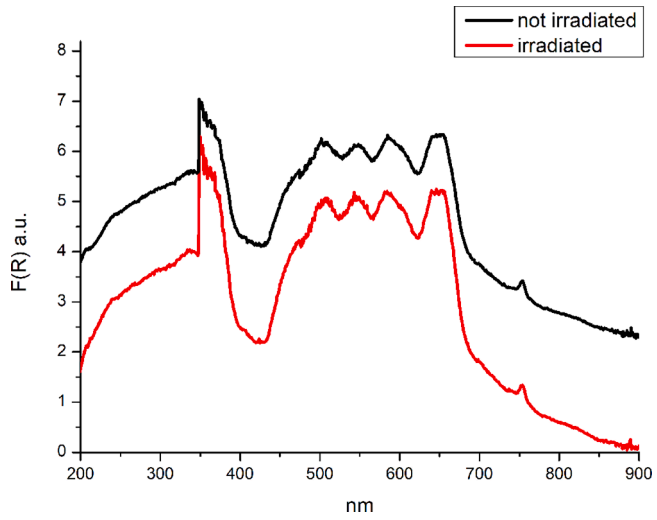

Fig. 2. UV–Vis absorbtion spectra of solid HTPP before and after irradiation.

techniques both in solution and in solid state.

3.1. SHG measurements

Powders of Co-TPP and sucrose were ground separately in an agate mortar for the same length of time and solid particles with sizes in the nano-scale magnitude were obtained. The ground powders were sealed into capillary tubes and irradiated with the 1.907 μm Raman shifted radiation of a Nd:YAG pulsed laser, to measure the SHG efficiency using sucrose as standard. The initial efficiency of the Co-TPP sample was of the same order of that of the sucrose, but, surprisingly, under laser irradiation, it gradually increased reaching, after few minutes, a plateau at a value about fifty times with respect to the initial one. By visually analyzing the powders in the capillaries, a darker spot was observed in correspondence of the point where the laser hit the samples. By repeating the measurement on the same spot, a stable SHG of about fifty times that of sucrose was measured; however, by moving the capillary on the not-irradiated powder, the same behavior of increasing of SHG under irradiation was again observed.

Even if the H_2TPP crystallizes in the centrosymmetric $P\bar{1}$ space group [43], and thus no SHG property is expected, also its SHG behavior was analyzed in the same conditions. In this case, the SHG signal remains null also after several minutes under irradiation.

3.2. UV–VIS, IR and MS analysis in solution

To investigate a possible photodegradation process, the Co-TPP in dichloromethane solution was analyzed before and after irradiation, using UV–VIS absorption and emission, FIR and ESI-MS spectrometry. Table 1 reports the main bands that characterize the UV–VIS absorption and emission spectra in dichloromethane. The whole spectra and a brief description are reported in the Supporting Information (Figs. S4–S7). Under the experimental conditions employed, the fluorescence signals for Co-TPP cannot be detected, as was the case with similar Cu-porphyrinate complexes [44].

No changes in the profiles are observable in the corresponding spectra. The IR and the ESI mass spectra (positive ion mode) of the H_2TPP and the Co-TPP complex, before and after irradiation with the Nd:YAG pulsed laser, are reported in Figs. S8–S13. Also in these cases, no significant changes in the profiles are perceptible before and after laser irradiation. In conclusion, the spectroscopic characterization does not evidence differences before and after irradiation with the Nd:YAG pulsed laser, and so we can exclude the occurrence of photodegradation.

3.3. Powder X-ray diffraction (XRPD)

Since the photo-degradation phenomenon was excluded by the spectroscopic characterization in solution, we considered the hypothesis of a possible phase transition or partial amorphization of the powder under the laser beam. In Fig. 1 are reported the XRPD patterns of the compound both before and after irradiation. The formation of a different crystalline phase after irradiation would change completely the peaks positions and intensities, while the amorphization process should reduce the intensities and enlarge the peaks. Thus, in each powder sample, an equal amount of ZnO as standard was mixed and the patterns were scaled on its higher intense peak: an eventual lowering of the intensity of the peaks of the Co-TPP complex with respect to the ZnO would indicate a lowering of the crystalline amount in the powders.

Fig. 1 evidences that no structural modifications or amorphization occur after irradiation in all compounds, since the relative intensities of their peaks with respect to ZnO remain unaltered. These results indicate

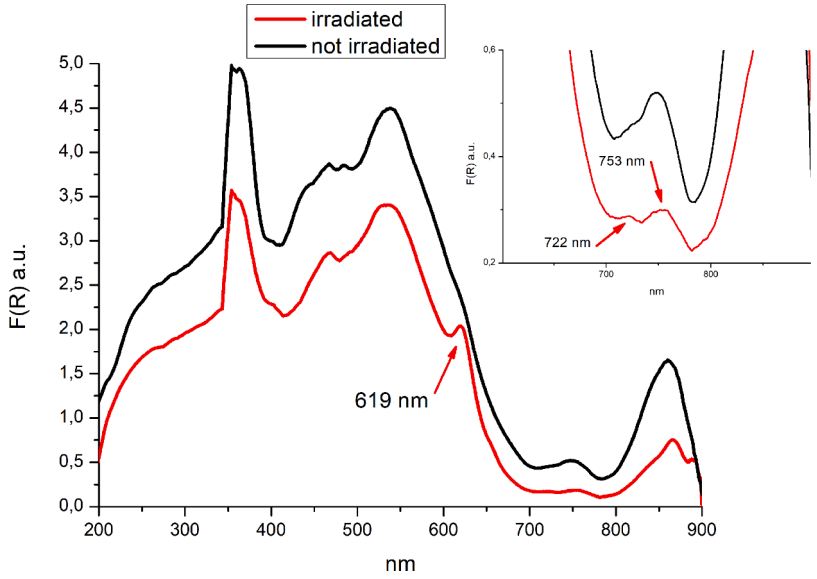

Fig. 3. UV–Vis absorption spectra of solid Co-TPP before and after irradiation. Differences were evidenced with arrows.

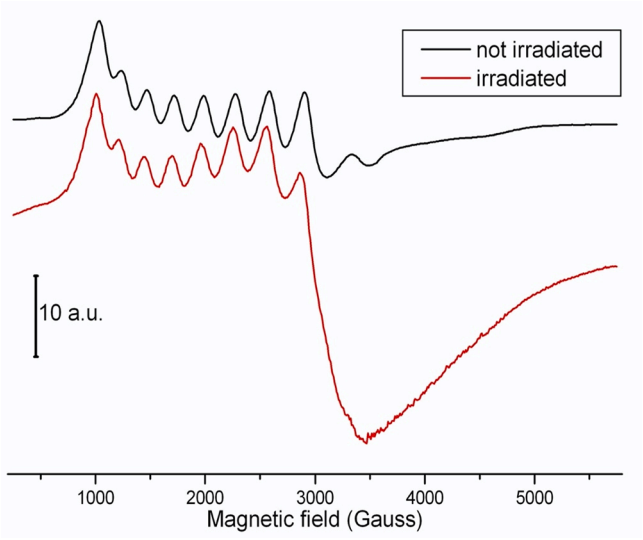

Fig. 4. EPR spectra of Co-TPP at 77 K before and after irradiation.

a strong chemical and structural stability of the Co-TPP porphyrinates to the irradiation with the Nd:YAG pulsed laser beam. This fact suggests that the cause of the remarkable increasing of the SH signal may be due to changes in the electronic and/or spin state induced by the laser beam. In order to further indagate a possible imperceptible variation of the structure, we attempted to irradiate a single crystal: surprisingly it blew up quite immediately after the irradiation, and it was divided into many crystalline fragments that were scattered in the capillary.

3.4. Magnetic balance

Three different Co-TPP samples were measured before and after irradiation and their magnetic moments were determined. In addition, six different measurements were made on one of the irradiated samples at one-week intervals. The results of the measurements on the non-irradiated samples are consistent with the literature data, which attribute a low spin state to the Co-TPP, since the measured magnetic moment lies between 2.0 and 2.8 BM. Instead, the irradiated Co-TPP samples show much higher magnetic moments, lying between 5.3 and 8.2 BM. Measurements carried out at regular time intervals have shown that the magnetic property is conserved over time.

These results demonstrate that during the laser irradiation of the samples takes place a change of the spin state and that they are excited into a high spin state or to a higher spin state. Magnetic moment values vary in a range corresponding to 3–6 unpaired electrons.

3.5. Experimental solid state UV–VIS absorption and EPR spectra

The powders of H_2TPP and Co-TPP, before and after irradiation, were analyzed with UV–VIS absorption end EPR spectra in the solid state. Fig. 2 reports the spectra of H_2TPP in the solid state before and after irradiation, which evidences no changes both in the number and in the wavelength of the bands due to irradiation, in agreement with the SHG experimental measurements.

Instead, in the spectra of Co-TPP before and after laser irradiation (Fig. 3) some differences are observed: in the irradiated sample, a new peak appears at 619 nm while only a slight shoulder is observed in the non-irradiated sample. Moreover, the band between 700 and 780 nm in the non-irradiated sample splits into two peaks at 722 and 753 nm, respectively.

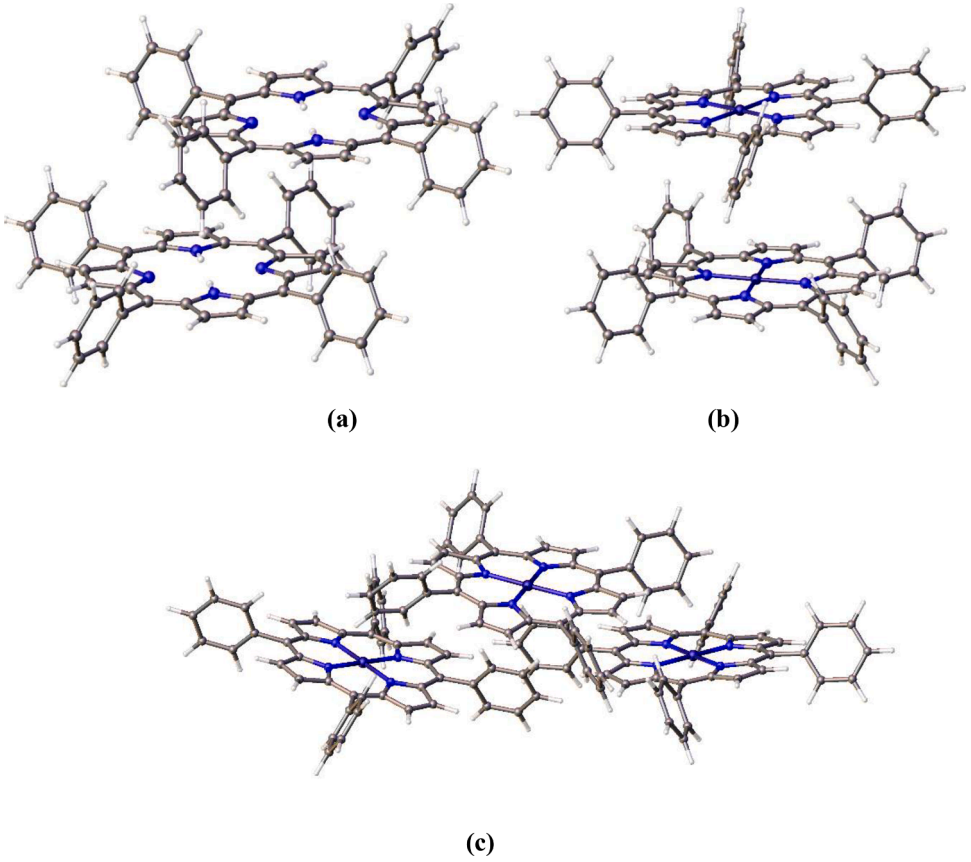

Fig. 5. Fragments H_2TPP (a) and Co-TPP (b) composed of two porphyrins rings and fragment composed of three rings (c) selected from the X-ray structure.

Table 2
Relevant distances (Å) around the metal atom for Co-TPP from X-ray data and B3LYP/6–31G(d) calculations. All theoretical distances are averaged for the chemically equivalent bonds of the fragments.

	Co-TPP XRD	Co-TPP 2 rings	Co-TPP 3 rings
Co-N1[i]	1.949(2)	1.995	2.051
Co-N1[ii]	1.949(2)	1.993	2.051
Co-N1[iii]	1.949(2)	1.993	2.051
Co-N1[iv]	1.949(2)	1.994	2.051

[i] 1-X,1-Y,-Z;
[ii] -3/2-Y,1/2 + *X*,−1/2-Z;
[iii] -2-X,−1-Y,+*Z*;
[iv] -1/2 + *Y*,−3/2-X,−1/2-Z.

Table 3
Relevant bond angles (degree) around the metal atom for Co-TPP from X-ray data and B3LYP/6–31G(d) calculations. All theoretical angles are averaged for the chemically equivalent bonds of the fragments.

	Co-TPP XRD	Co-TPP 2 rings	Co-TPP 3 rings
N1[1]-Co1-N1[2]	178.75(12)	179.28	178.90
N1[2]-Co1-N1	90.006(2)	89.93	90.19
N1[1]-Co1-N1[3]	90.007(1)	90.05	90.19
N1[3]-Co1-N1	178.75(12)	179.40	178.89
N1[1]-Co1-N1	90.007(2)	89.99	89.82
N1[2]-Co1-N1[3]	90.007(2)	90.03	89.82

[1] –3/2-Y,1/2 + *X*,−1/2-Z.
[2] –1/2 + *Y*,−3/2-X,−1/2-Z.
[3] –2-X,−1-Y,+*Z*.

Table 4
Root mean square deviations RMSD (Å) of the atomic positions with respect to the mean plane of the porphyrin ring for H_2TPP and Co-TPP fragments.

	H_2TPP 2 rings	Co-TPP 2 rings	Co-TPP 3 rings
B3LYP [a]	0.047 - 0.060	0.094 - 0.105	0.095 - 0.145 - 0.133
XRD	0.069[29]	0.245	0.245

[a] The multiple values correspond to the deviation from the root mean square of the different rings of the same fragment.

In Fig. 4 are shown the EPR spectra of Co-TPP before and after irradiation. The spectrum before irradiation is comparable with previous data reported in literature [45] and consistent with a Co(II) low-spin system ($S = 1/2$ and $I = 7/2$). Spectral simulation with the Bruker Anisotropic SpinFit software confirms for Co-TPP before irradiation an axial symmetry with a slight rhombic distortion ($g_{\perp} = 3.34$; $g_{//} = 1.83$). After irradiation, this pattern is partially substituted by a very large isotropic signal, centered at $g = 2.40$, indicating a partial, but evident, modification of the Co-TPP properties. Unfortunately, the absence of a hyperfine structure or other specific features in the EPR signal of the irradiated sample does not allow to attribute these changes with certainty, but they are probably related to the modification in the spin state of the system, in agreement to the results of the magnetic susceptibility measurements.

3.6. Computational results

Theoretical calculations were performed taking into account that the experimental SHG measurements are carried out on crystalline powders of the nanoparticles' size. To better simulate the size of the nanoparticle, small fragments were selected starting from the X-ray structures. These models allow to take into account the structural distortion that the surface forces can induce at the nanoscale level. The fragments are composed of two or three rings, cut from the crystallographic structural data to evaluate the effect of the fragment size on the hyperpolarizability and optical susceptibility. Fig. 5 shows the fragments with two and three rings of H_2TPP and Co-TPP. For each fragment, calculations were performed on the lowest spin state, chosen on the basis of experimental data [46], or first calculating several multiplicities and then choosing the structure with the lowest energy. For Co-TPP the lowest spin state is the doublet. The same type of calculations was performed for the H_2TPP, on a fragment composed of two rings selected from the crystal structure downloaded from the Cambridge Crystal Structural Database (CSD) [43]. Since sucrose is the reference compound for the SHG measurements, the same type of calculations was carried out also on a model of sucrose, composed of four sucrose units selected from the crystal structure downloaded from the CSD [47].

In Tables 2 and 3 are reported the most relevant geometrical parameters, compared to the corresponding X-ray structural data (the Cartesian coordinates of all fragments are reported in Tables S3–S9. In the fragments of the Co-TTP complex the bond differences are small and range from 0.046 Å, for the fragment with two rings, to a maximum of 0.1 Å for the fragment with three rings; about the bond angles, they are very similar to the experimental data, for all fragments.

In Table 4 are reported the root mean-square deviations (RMSD) of the atomic positions, calculated with the Olex2 software, with respect to the mean plane of the porphyrin ring (that include all the N atoms and

Table 5
Computed dipole moments μ (Debye), mean polarizabilities <α> (a.u.), first static hyperpolarizabilities β_{tot} (10^{-30} cm^5esu^{-1}), second order susceptibilities $\chi^{(2)}$ (pmV^{-1}), second order susceptibilities ratios with respect to sucrose values.

	H_2TPP 2 rings	Co-TPP 2 rings	Co-TPP 3 rings
μ	0.000	0.517	0.708
<α>	1214.6	1232.8	1888.8
β_{tot}	0.0	2.3	2.6
$\chi^{(2)}$	0.0	0.4	0.3
$\chi^{(2)}/\chi^{(2)}_{sucrose}$	0.0	0.2	0.2

Table 6
Relevant distances (Å) around the metal atom for Co-TPP of the fragments with two and three rings in different spin excited states, calculated at the B3LYP/6–31G(d) level. The number of unpaired electrons in the fragments is given in parenthesis. All theoretical distances are averaged for the chemically equivalent bonds of the fragments.

	2rings (6)	2rings (8)	2rings (10)	3rings (15)
Co-N1[i]	2.049	2.051	2.060	2.060
Co-N1[ii]	2.050	2.058	2.062	2.064
Co-N1[iii]	2.051	2.050	2.061	2059
Co-N1[iv]	2.052	2.058	2.061	2.065

[i] 1-X,1-Y,-Z;
[ii] -3/2-Y,1/2 + *X*,−1/2-Z;
[iii] -2-X,−1-Y,+*Z*;
[iv] -1/2 + *Y*,−3/2-X,−1/2-Z.

Table 7
Relevant bond angles (degree) around the metal atom of the fragments with two and three rings in different spin excited states calculated at the B3LYP/6–31G(d) level. The number of unpaired electrons in the fragments is given in parenthesis. All theoretical angles are averaged for the chemically equivalent bonds of the fragments.

	2rings (6)	2rings (8)	2rings (10)	3rings (15)
N1[1]-Co1-N1[2]	179.30	178.90	179.50	178.90
N1[2]-Co1-N1	90.05	89.85	90.00	90.01
N1[1]-Co1-N1[3]	89.88	90.10	89.94	90.07
N1[3]-Co1-N1	179.50	179.8	178.99	178.65
N1[1]-Co1-N1	90.00	90.00	90.00	89.88
N1[2]-Co1-N1[3]	90.08	89.95	89.90	90.07

[1] –3/2-Y,1/2 + *X*,−1/2-Z.
[2] –1/2 + *Y*,−3/2-X,−1/2-Z.
[3] –2-X,−1-Y,+*Z*.

Table 8
Dipole moments μ (Debye), mean polarizabilities <α> (a.u.), first static hyperpolarizabilities β_{tot} (10^{-30} cm^5esu^{-1}) computed for Co-TPP on optimized geometries of fragments with several excited spin states.

Unpaired electrons in the fragment of CoTPP	6[a]	8[a]	10[a]	15[b]
μ	0.631	0.125	0.408	0.722
<α>	1259.7	1272.5	1332.9	2059.3
β_{tot}	2.7	11.1	17.9	18.9

[a] Fragment with two rings.
[b] Fragment with three rings.

Table 9
Theoretical and experimental electronic transitions (nm). The width of the bands is reported in parenthesis.

	Experimental	Theoretical
Soret bands	353 (348–398)	374 (369–398)
	536	(418–493)
Q bands		522 (521–523)
	619	(597–599)
	(712–782)	(701–712)
		(777–780)
	(784–895)	(900–908)

all C atoms except those of the phenyl rings) in the optimized fragments and obtained from XRD data.

As it can be observed in Table 4, for H_2TPP the RMSD is close to the experimental values, while for Co-TPP the calculations provide a more planar structure. On the other hand, in Co-TPP the calculated Co-N bond distances are longer than the experimental ones (Table 2). These results confirm that the Co-N bond distances have a great effect on the conformation of the porphyrin core as observed by Madura et al. [48]: in fact, the greater is the length of the Co-N bond, the greater is the deviation from planarity of the porphyrin core.

In Table 5 are reported for all fragments the computed values of the dipole moment μ, the mean polarizability α, and an estimate of the intrinsic molecular hyperpolarizability (β) in the absence of any resonance effect represented by a third rank tensor. The twenty-seven components of the 3D matrix can be reduced to ten components according to Kleinman symmetry. The Gaussian16 output file provides the main ten components (β_{xxx}, β_{xxy}, β_{xyy}, β_{yyy}, β_{xxz}, β_{xyz}, β_{yyz}, β_{xzz}, β_{yzz}, and β_{zzz}), whose values for the studied compounds are given in Tables S10–S15. The magnitude of the total first hyperpolarizability (β_{tot}) can be defined as,

$$\beta_{tot} = \sqrt{\left(\beta_{xxx} + \beta_{xyy} + \beta_{xzz}\right)^2 + \left(\beta_{xxy} + \beta_{yyy} + \beta_{yzz}\right)^2 + \left(\beta_{xxz} + \beta_{zyy} + \beta_{zzz}\right)^2} \quad (3)$$

The relationship between the macroscopic second-order susceptibility, the quantity correlated to the second harmonic intensity, and the microscopic hyperpolarizability is given by Eq. (4) [49]:

$$\chi^{(2)} = \beta_{tot} NF \quad (4)$$

where N is the number of particles per unit volume and F is the local field factor. F depends upon the crystal symmetry and is related to the crystal's refractive index. Values between 1 and 2 are generally reported and, in particular for saccharides, this value range between 1.5 and 1.6 [50].

We assume $F = 1$ since our interest is focused on the trend of the ratio $\chi^{(2)}/\chi^{(2)}_{\text{sucrose}}$. The ratios between the second-order susceptibility of the compounds and that of sucrose is also reported, together with the ratios between the corresponding SHG intensities, in order to compare the computational results with the experimental measurements.

All Co-TPP fragments including porphyrin have rather high polarizability values, but very low hyperpolarizability and optical susceptibility and all values are of the same order of magnitude. However, the ratios of optical susceptibility with respect to sucrose are all extremely low. These results confirm that both the porphyrin and the Co-TPP show low SHG in agreement with the experimental SHG efficiencies at the beginning of the irradiation with the Nd:YAG pulsed laser.

Considering the results obtained with the magnetic balance and the magnetic moments of the irradiated Co-TPP, we performed geometry optimizations at the B3LYP/6–31G(d) of the fragment with two and tree rings in different spin excited states, in order to evaluate the variation of the hyperpolarizability (β) as a function of the number of unpaired electrons of the system. The main geometrical parameters are shown in Tables 6, 7 and the values of the dipole moment, polarizability and hyperpolarizability as a function of the number of unpaired electrons are shown in Table 8. All geometrical parameters and all components of vectors and tensors are reported in Table S4–S6, S8, S11–S13, S15.

The results of Tables 6 and 7 show that the geometry parameters of the excited spin states are very similar to the geometry of the ground state, in agreement with the experimental data that do not detect structural changes for the irradiated sample.

Data in Table 8 show that both the dipole moment and the polarizability values have small changes as a function of the spin state, in the fragment with two rings, while the hyperpolarizability changes by an order of magnitude from 2, 3 to 4, 5 unpaired electrons. This result is in agreement with the experimental data of the magnetic balance, in which the irradiated sample has a high SHG emission and a rather high magnetic moment compatible with excited spin states.

TDDFT calculations performed on the fragment with three rings in the ground state yielded a UV spectrum that is generally in good agreement with the peak positions of the experimental spectrum (see Table 9 and Fig. 3). Differences are observed due to the presence of electronic transitions at wavelengths between 597 and 599 nm with a change in the spin state of the system from three to four unpaired electrons and with zero oscillator strength. Only a slight shoulder appears in the experimental spectrum of the sample not irradiated, at the same wavelengths. It is interesting to note that in the experimental spectrum of the irradiated sample a more intense peak appears at the same wavelengths. Furthermore, a splitting of the band between 700 and 780 nm is also observed in the theoretical TDDFT spectrum. The spectrum has two different ranges of electronic transitions, 708 -712 nm and 777-780 nm, both with spin state change and zero oscillator strength.

4. Conclusions

In this work we observed a peculiar SHG behavior of the solid Co derivative of the 5,10,15,20-tetraphenylporphyrin, and we attempted to understand what occurs during the irradiation with the Nd:YAG pulsed laser, both through experimental analysis and theoretical calculations. Mass spectrometry, absorption, emission and vibrational spectroscopies in solution, before and after irradiation, do not evidence any chemical degradation or transformation of the sample. The XRPD analysis on the crystalline powder allows to exclude an amorphization process during laser irradiation. The theoretical calculations on small fragments of Co-TPP simulate appropriately the structural features of the complexes and their initial experimental SHG responses. Undoubtedly, the insertion of the metal in the porphyrin ring, inducing a remarkable distortion of the former, as observed in the XRD structures and in the theoretical calculations, has a role in the modification of the SHG property of the porphirinate, since in the free porphyrin this phenomenon was not observed. In this work, it was hypothesized that the enhancement of the SHG efficiencies of the Co-TPP complex is imputable to an electronic or spin transition that occurs when the Co-porphyrinate was irradiated. In fact, the magnetic moment measurements on the irradiated fragments show a substantial change in the spin state of the samples. This result is

confirmed by the observed differences in the EPR spectrum of the sample before and after irradiation. Furthermore, the UV–VIS spectrum of the irradiated sample shows differences in the number of observed peaks, that can be attributed to a greater number of electronic transitions.

The theoretical calculations carried out on the fragments in different excited spin states confirm the result of the magnetic balance: in fact, an increase in hyperpolarizability, an intrinsic property linked to SHG emission, is observed as a function of the increase in the number of unpaired electrons.

CRediT authorship contribution statement

Paola Antoniotti: Conceptualization, Methodology, Software, Validation, Formal analysis, Investigation, Resources, Data curation, Writing – original draft, Writing – review & editing, Visualization, Supervision, Project administration. **Carlo Canepa:** Validation, Investigation, Resources, Data curation, Writing – review & editing. **Elena Cariati:** Validation, Investigation, Resources, Data curation, Writing – review & editing. **Alma Cioci:** Methodology, Software, Validation, Formal analysis, Investigation, Resources, Data curation, Writing – review & editing. **Enzo Laurenti:** Validation, Investigation, Resources, Data curation, Writing – review & editing. **Domenica Marabello:** Validation, Formal analysis, Investigation, Resources, Data curation, Writing – original draft, Writing – review & editing, Visualization, Supervision, Project administration. **Giorgio Volpi:** Validation, Investigation, Resources, Data curation, Writing – review & editing. **Paola Benzi:** Validation, Formal analysis, Investigation, Resources, Data curation, Writing – review & editing, Visualization, Project administration.

Declaration of Competing Interest

The authors declare that they have no known competing financial interests or personal relationships that could have appeared to influence the work reported in this paper.

Data availability

Data will be made available on request.

Aknowledgement

Financial support from MIUR (Ministero dell'Istruzione, dell'Università e della Ricerca) is acknowledged.

Supplementary materials

Supplementary material associated with this article can be found, in the online version, at doi:10.1016/j.molstruc.2023.136340.

References

[1] H. Lee, K.I. Hong, W.D. Jang, Design and applications of molecular probes containing porphyrin derivatives, Coord. Chem. Rev. 354 (2018) 46–73.
[2] A. Mahmood, J.Y. Hu, B. Xiao, A. Tang, X. Wang, E. Zhou, Recent progress in porphyrin-based materials for organic solar cells, J. Mater. Chem. A 6 (2018) 16769–16797.
[3] G. Pandey, R. Chaudhari, B. Joshi, S. Choudhary, J. Kaur, A. Joshi, Fluorescent biocompatible platinum-porphyrin–doped polymeric hybrid particles for oxygen and glucose biosensing, Sci. Rep. 9 (2019) 5029–5040.
[4] K. Norvaiša, M. Kielmann, M.O. Senge, Porphyrins as Colorimetric and photometric biosensors in modern bioanalytical systems, ChemBioChem 21 (2020) 1–16.
[5] M. Imran, M. Ramzan, A.K. Qureshi, M.A. Khan, M. Tariq, Emerging applications of porphyrins and metalloporphyrins in biomedicine and diagnostic magnetic resonance imaging, Biosensors 8 (2018) 95–111.
[6] S. Chandra, C. Mende, D. Bahadur, A. Hildebrandt, H. Lang, Fabrication of a porphyrin-based electrochemical biosensor for detection of nitric oxide released by cancer cells, J. Solid State Electrochem. 19 (2015) 169–177.
[7] M.O. Senge, M. Fazekas, E.G.A. Notaras, W.J. Blau, M. Zawadzka, O.B. Locos, E. M. Ni Mhuircheartaigh, Nonlinear optical properties of porphyrins, Adv. Mater. 19 (2007) 2737–2774.
[8] F. Tessore, A. Orbelli Biroli, G. Di Carlo, M. Pizzotti, Porphyrins for second order nonlinear optics (NLO): an intriguing history, Inorganics 6 (2018) 81.
[9] K.S. Suslick, C.T. Chen, G.R. Meredith, L.T. Cheng, Push-pull porphyrins as nonlinear optical materials, J. Am. Chem. Soc. 114 (1992) 6928–6930.
[10] X. Liu, D. Wang, H. Gao, Z. Yang, Y. Xing, H. Cao, W. He, H. Wang, J. Gu, H. Hu, Nonlinear optical properties of symmetrical and asymmetrical porphyrin derivatives with click chemistry modification, Dyes Pigm. 134 (2016) 155–163.
[11] S. Yamada, K. Kuwata, H. Yonemura, T. Matsuo, Second-order nonlinear optical properties of amphiphilic porphyrins in Langmuir-Blodgett monolayer assemblies, J. Photochem. Photobiol. A Chem. 87 (1995) 115–119.
[12] K. Sendhil, C. Vijayan, M.P. Kothiyal, Nonlinear optical properties of a porphyrin derivative incorporated in Nafion polymer, Opt. Mater. 27 (2005) 1606–1609 (Amst).
[13] A. Khadria, J. Fleischhauer, I. Boczarow, J.D. Wilkinson, M.M. Kohl, H. L. Anderson, Porphyrin dyes for nonlinear optical imaging of live cells, iScience 4 (2018) 153–163.
[14] J.E. Reeve, H.A. Collins, K.D. Mey, M.M. Kohl, K.J. Thorley, O. Paulsen, K. Clays, H.L. Anderson, Amphiphilic porphyrins for second harmonic generation imaging, J. Am. Chem. Soc. 131 (8) (2009) 2758–2759.
[15] X. Liu, D. Wang, H. Gao, Z. Yang, Y. Xing, H. Cao, W. He, H. Wang, J. Gu, H. Hu, Nonlinear optical properties of symmetrical and asymmetrical porphyrin derivatives with click chemistry modification, Dyes Pigm. 134 (2016) 155–163.
[16] M. Pizzotti, E. Annoni, R. Ugo, S. Bruni, S. Quici, P. Fantucci, M. Bruschi, G. Zerbi, M. Del Zoppo, Multitechnique investigation of the second order NLO response of a 10,20-diphenylporphyrinato nickel(II) complex carrying a phenylethynyl based push–pull system in the 5- and 15- positions, J. Porphyrins Phtalocyanines 8 (2004) 1311–1324.
[17] F. Tessore, A. Orbelli Biroli, G. Di Carlo, M. Pizzotti, Porphyrins for second order nonlinear optics (NLO): an intriguing history, Inorganics 6 (2018) 81.
[18] E. Annoni, M. Pizzotti, R. Ugo, S. Quici, T. Morotti, M. Bruschi, P. Mussini, Synthesis, electronic characterization and significant second-order non-linear optical responses of meso-tetraphenylporphyrins and their ZnII complexes carrying a push or pull group in the β pyrrolic position, Eur. J. Inorg. Chem. (2005) 3857–3874.
[19] T. Morotti, M. Pizzotti, R. Ugo, S. Quici, M. Bruschi, P. Mussini, S. Righetto, Electronic characterisation and significant second-order NLO response of 10,20-diphenylporphyrins and their Zn-II complexes substituted in the meso position with pi-delocalised linkers carrying push or pull groups, Eur. J. Inorg. Chem. 9 (2006) 1743–1757.
[20] S.M. Lecours, H.W. Guan, S.G. Dimagno, C.H. Wang, M.J. Therien, Push-pull arylethynyl porphyrins: new chromophores that exhibit large molecular first-order hyperpolarizabilities, J. Am. Chem. Soc. 118 (1996) 1497–1503.
[21] K. De Mey, K. Clays, M.J. Therien, D.N. Beratan, I. Asselberghs, Analysis of the unusual wavelength dependence of the first hyperpolarizability of porphyrin derivatives, in: Proceedings of the SPIE - Linear and Nonlinear Optics of Organic Materials X, 2010, 777403, https://doi.org/10.1117/12.859819.
[22] D. Marabello, P. Antoniotti, P. Benzi, C. Canepa, E. Diana, L. Operti, L. Mortati, M. P. Sassi, Non-linear optical properties of β-D-fructopyranose calcium chloride MOFs: an experimental and theoretical approach, J. Mater. Sci. 50 (2015) 4330–4341.
[23] D. Marabello, P. Antoniotti, P. Benzi, C. Canepa, L. Mortati, M.P. Sassi, Synthesis, structure and non-linear optical properties of new isostructural β-D-fructopyranose alkaline halide metal–organic frameworks: a theoretical and an experimental study, Acta Crystallogr. B Struct. Sci. Cryst. Eng. Mater. 73 (2017) 737–743.
[24] D. Marabello, P. Antoniotti, P. Benzi, E. Cariati, L.Lo Presti, C. Canepa, Developing new SrI_2 and β-D-fructopyranose-based metal–organic frameworks with nonlinear optical properties, Acta Crystallogr. B Struct. Sci. Cryst. Eng. Mater. 75 (2019) 210–218.
[25] Y.R. Shen, The Principles of Nonlinear Optics, Wiley, New York, 1984.
[26] G.S. Girolami, T.B. Rauchfuss, R.J. Angelici, Synthesis and Technique in Inorganic Chemistry, 3rd ed., University Science Books: Melville, NY, 1999. ISBN 978-0-935702-48-4.
[27] CrysAlisPro (2014). Agilent technologies, version 1.171.37.31 (release 14-01-2014 CrysAlis171. NET, compiled Jan 14 2014,18:38:05.
[28] G.M. Sheldrick, SHELXT-integrated space-group and crystal-structure determination, Acta Cryst. A71 (2015) 3–8.
[29] G.M. Sheldrick, Crystal structure refinement with SHELXL, Acta Cryst. C71 (2015) 3–8.
[30] O.V. Dolomanov, L.J. Bourhis, R.J. Gildea, J.A.K. Howard, H. Puschmann, Complete structure solution, refinement and analysis program, J. Appl. Cryst. 42 (2009) 339–341.
[31] Gaussian 16, Revision C.01, M.J. Frisch, G.W. Trucks, H.B. Schlegel, G.E. Scuseria, M.A. Robb, J.R. Cheeseman, G. Scalmani, V. Barone, G.A. Petersson, H. Nakatsuji, X. Li, M. Caricato, A.V. Marenich, J. Bloino, B.G. Janesko, R. Gomperts, B. Mennucci, H.P. Hratchian, J.V. Ortiz, A.F. Izmaylov, J.L. Sonnenberg, D. Williams-Young, F. Ding, F. Lipparini, F. Egidi, J. Goings, B. Peng, A. Petrone, T. Henderson, D. Ranasinghe, V.G. Zakrzewski, J. Gao, N. Rega, G. Zheng, W. Liang, M. Hada, M. Ehara, K. Toyota, R. Fukuda, J. Hasegawa, M. Ishida, T. Nakajima, Y. Honda, O. Kitao, H. Nakai, T. Vreven, K. Throssell, J.A. Montgomery, Jr., J.E. Peralta, F. Ogliaro, M.J. Bearpark, J.J. Heyd, E.N. Brothers, K.N. Kudin, V.N. Staroverov, T.A. Keith, R. Kobayashi, J. Normand, K. Raghavachari, A.P. Rendell, J.C. Burant, S.S. Iyengar, J. Tomasi, M. Cossi, J.M. Millam, M. Klene, C. Adamo, R. Cammi, J.W.

Ochterski, R.L. Martin, K. Morokuma, O. Farkas, J.B. Foresman, and D.J. Fox, Gaussian, Inc., Wallingford CT, 2016.
[32] H.B. Schlegel, C. Daudel, Computational Theoretical Organic Chemistry, Reidel, Dordrecht, 1981, p. 129, edited by I. G. Csizsmadia and R. Daudel.
[33] H.B. Schlegel, An efficient algorithm for calculating ab initio energy gradients using s, p Cartesian Gaussians, J. Chem. Phys. 77 (1982) (1982) 3676–3681.
[34] H.B. Schlegel, Optimization of equilibrium geometries and transition structures, J. Comput. Chem. 3 (1982) 214–218.
[35] A.D. Becke, Density-functional exchange-energy approximation with correct asymptotic behavior, Phys. Rev. A 38 (6) (1988) 3098–3100.
[36] A.D. Becke, Density-functional thermochemistry. III. the role of exact exchange, J. Chem. Phys. 98 (7) (1993) 5648–5652.
[37] W.J. Hehre, L. Radom, P.Vr Schleyer, J.A. Pople, Ab Initio Molecular Orbital Theory, Wiley, New York, 1986.
[38] W.R. Wadt, P.J. Hay, Ab initio effective core potentials for molecular calculations. Potentials for the transition metal atoms *Sc* to Hg, J. Chem. Phys. 82 (1985) 270–283.
[39] D.F. Parsons, B.W. Ninham, Ab initio molar volumes and Gaussian radii, J. Phys. Chem. A 113 (6) (2009) 1141–1150, https://doi.org/10.1021/jp802984b. PMID19140766.
[40] R. Bauernschmitt, R. Ahlrichs, Treatment of electronic excitations within the adiabatic approximation of time dependent density functional theory, Chem. Phys. Lett. 256 (1996) 454–464, https://doi.org/10.1016/0009-2614(96)00440-X.
[41] R.E. Stratmann, G.E. Scuseria, M.J. Frisch, An efficient implementation of time-dependent density-functional theory for the calculation of excitation energies of large molecules, J. Chem. Phys. 109 (1998) 8218–8224, https://doi.org/10.1063/1.477483.
[42] S.K. Kurtz, T.T. Perry, A powder technique for the evaluation of nonlinear optical materials, J. Appl. Phys. 39 (1968) 3798–3813.
[43] S.J. Silvers, A. Tulinsky, The crystal and molecular structure of triclinic tetraphenylporphyrin, J. Am. Chem. Soc. 89 (1967) 3331–3337.
[44] W. Zheng, N. Shan, L. Yu, X. Wang, UV–visible, fluorescence and EPR properties of porphyrins and metalloporphyrins, Dyes Pigm. 77 (2008) 153–157.
[45] D. Skrzypek, I. Madejska, J. Habdas, The characterization of cobalt(II) derivatives of selected substituted meso-tetraphenyl and tetrapyridyl porphyrins by EPR spectroscopic study, Solid State Sci. 9 (2007) 295–302, https://doi.org/10.1016/j.solidstatesciences.2006.12.005.
[46] M.S. Liao, S. Scheiner, Electronic structure and bonding in metal porphyrins, metal=Fe,Co,Ni,Cu,Zn, J. Chem. Phys. 117 (2002) 205–218.
[47] G.M. Brown, H.A. Levy, Further refinement of the structure of sucrose based on neutron-diffraction data, Acta Crystallogr. B29 (1973) 790–797.
[48] P. Madura, W.R. Scheidt, Stereochemistry of low-spin cobalt porphyrins, Inorg. Chem. 15 (12) (1976) 3182–3184.
[49] R.W. Boyd, Nonlinear Optics, 3rd ed., Academic Press: Philadelphia, 2008. ISBN: 978-0-12-369470-6.
[50] R.R. Choudhury, R. Chitra, Investigation of hydrogen bond effects on the hyperpolarizability of 2-Aminopyridinium maleate (2APM) complex and determining the non-linear optical susceptibility of the molecular crystal of 2APM, Mol. Phys. 109 (13) (2011) 1701–1708, https://doi.org/10.1080/00268976.2011.587458.